This is a preprint, the final version is subject to change, of the American Mineralogist (MSA)
Cite as Authors (Year) Title. American Mineralogist, in press.
DOI: http://dx.doi.org/10.2138/am-2018-6164

REVISION 1: A common origin for Thai/Cambodian rubies and blue and violet sapphires from Yogo Gulch, Montana, USA?

Aaron C. Palke*[1,2,3], Jacqueline Wong[3], Charles Verdel[3], and Janaína N. Ávila[4]

1. Gemological Institute of America, Carlsbad, CA 92008, USA
2. Queensland Museum, Brisbane, QLD 4011, Australia
3. University of Queensland, St. Lucia, QLD 4072, Australia
4. The Australian National University, Canberra, ACT 2601, Australia

*apalke@gia.edu

Abstract

A wide number of genetic models have been proposed for volcanically-transported ruby and sapphire deposits around the world. In this contribution we compare the trace element chemistry, mineral and melt inclusions, and oxygen isotope ratios in blue to reddish-violet sapphires from Yogo Gulch, Montana, USA with rubies from the Chantaburi-Trat region of Thailand and the Pailin region of Cambodia. The similarities between Thai/Cambodian rubies and Yogo sapphires suggest a common origin for gem corundum from both deposits. Specifically, we advance a model whereby sapphires and rubies formed through a peritectic melting reaction when the lamprophyre or basalts that transported the gem corundum to the surface partially melted Al-rich lower crustal rocks. Furthermore, we suggest the protolith of the rubies and sapphires was an anorthosite or, in the case of Thai/Cambodian rubies, an anorthosite subjected to higher pressures and converted into a garnet-clinopyroxenite. In this model the rubies and sapphires are rightfully considered to be xenocrysts in their host basalts or lamprophyre; however, in this scenario they are not "accidental" xenocrysts but their formation is intimately and directly linked to the magmas that transported them to the surface. The similarities in these gem corundum deposits suggests that the partial melting, non-accidental xenocryst model may be more

wide-reaching and globally important than previously realized. Importantly, in both cases the gem corundum has an ostensibly "metamorphic" trace element signature, whereas the presence of silicate melt (or magma) inclusions shows they ought to be considered to be "magmatic" rubies and sapphires. This discrepancy suggests that existing trace element discriminant diagrams intended to separate "metamorphic" from "magmatic" gem corundum ought to be used with caution.

Keywords: sapphire, ruby, Yogo Gulch, melt inclusions, corundum, gemology

Introduction:

Volcanically-hosted gem corundum deposits are widespread across the western Pacific margin (eastern Australia, southeast Asia, China, eastern Russia). There are also examples in northeast Russia, France, Slovakia, Africa, Scotland, and North and South America (see references in Giuliani et al. 2014; Hughes, 2014; Hughes et al. 2017). They mostly produce sapphires with minor ruby. However, the southeastern Asian nations of Thailand and Cambodia are important major historic producers of rubies [gem-quality corundum (α-Al_2O_3) colored red by Cr^{3+}] derived from basalts. While gem production in these areas has declined significantly in recent years, these two countries were major suppliers of gem corundum (especially ruby) during the 20th century. Rubies are found here in alluvial deposits in a region spanning the southern border between Thailand and Cambodia. In Thailand, the gems fields are found in the Chanthaburi-Trat area, while in Cambodia the gem-bearing deposits are in the Pailin region. In both cases, it is generally accepted that the rubies were transported to the surface by young Cenozoic alkali basalt volcanism (<3 Ma, Barr and MacDonald, 1981; Sutthirat et al. 1994). Yet, it is also accepted that the rubies are xenocrysts within the basalts and were transported from somewhere deep within the Earth. Genetic models for Thai/Cambodian rubies generally suggest they formed through high pressure metamorphism of (ultra)mafic rocks (Sutthirat et al. 2001; Saminpanya and Sutherland 2011). These gemfields have also produced a significant quantity of blue sapphires (gem-quality corundum colored by

Fe and Ti), which have distinct inclusion suites and trace element chemistry patterns indicating a different origin than the rubies. The Thai and Cambodian gem fields are generally very similar to other alluvial sapphire deposits associated with alkali basalt fields across the western Pacific margin. The main difference is the generally higher proportion of rubies found in Thailand and Cambodia relative to other major producers of gem corundum like Australia, which produce predominantly blue, green, and yellow sapphires (Graham et al. 2008). This study focuses only on Thai/Cambodian rubies, whereas sapphires from that region are not discussed. While many studies of ruby deposits focus on either the Chathaburi-Trat area in Thailand or the Pailin region in Cambodia, it is widely recognized that both gem-producing regions are essentially one single deposit straddling the border between the two countries. The rubies found in both countries are generally indistinguishable in terms of their trace element chemistry and inclusions suites, so in the rest of this contribution we will refer to these rubies simply as Thai/Cambodian rubies without distinguishing between the two.

Nearly on the other side of the world in Montana, USA is the Yogo Gulch sapphire deposit. Yogo sapphires are found in a primary deposit and are embedded in a lamprophyre dike. Similar to Thai/Cambodian rubies, Yogo sapphires were transported to the surface from somewhere deep within the Earth by this lamprophyre and they are considered to be xenocrysts in the dike. The Yogo lamprophyre is properly classified as a ouachitite and has been dated at 48.2 Ma (Gauthier 1995). Yogo sapphires are revered for their cornflower blue color, although a small proportion of sapphires are enriched in Cr and veer into the domain of violet sapphires to the rare red Yogo rubies.

What exactly do these seemingly disparate deposits of gem corundum have in common? Besides the fact that Thai/Cambodian rubies and Yogo sapphires were transported to the surface by relatively recent Cenozoic volcanism, on the surface there doesn't appear to be much linking them. Thai/Cambodian rubies are generally considered to have a "metamorphic" origin based on their trace element chemistry and inclusion suites (Sutthirat et al. 2001; Sutherland et al. 2002, 2003, 2008;

Saminpanya and Sutherland 2011). Yogo sapphires also have "metamorphic" trace element chemistry; however, Palke et al. (2016) noted the presence of Na- and Ca-rich glassy melt inclusions in Yogo sapphires, which suggest a magmatic origin instead. Based on their analysis, it was proposed that these sapphires formed through partial melting of an anorthite-plagioclase-rich protolith such as a troctolite or anorthosite when the Yogo lamprophyre intruded and temporarily pooled at the base of the crust. Importantly, melt inclusions have been reported in Thai/Cambodian rubies (Gübelin and Koivula 2008) which also suggests a magmatic origin for this deposit. The similar mineralogical and gemological properties of gem corundum from Yogo Gulch and Thailand/Cambodia was also recognized by Hughes et al. (2017) who suggested that these sapphires and rubies may have a similar origin. Hughes et al. (2017) noted simlilarities in their inclusion suites and the morphology of rough crystals. This study will analyze melt inclusions and trace element compositions of Thai/Cambodian rubies in order to test the hypothesis that they have a common genetic origin involving partial melting of an Al-rich protolith when basaltic or lamphrophyric magma intruded into or near the base of the crust. While this model has been proposed already for sapphires from Montana (Palke et al. 2016, 2017), its likely involvement in two seemingly unrelated deposits formed during different geological events suggests that this may be a more wide-reaching model for ruby and sapphire genesis than previously realized.

Analytical Methods:

Electron Probe MicroAnalysis

Electron Probe MicroAnalysis (EPMA) was performed at Caltech on a JEOL JXA-8200 with an accelerating voltage of 15 kV and a defocused beam of 10 μm and 10 nA to avoid alkali migration. When possible, melt inclusions were analyzed in several clean spots on a single inclusion with a reduced beam current of 5 nA or 2.5 nA. In all cases, repeat analyses with lower current gave identical results suggesting that alkali migration is not a problem for these glasses even with conditions of 10 μm and 10

nA. Standards include rhyolite glass VG-568 (Si), TiO_2 (Ti), anorthite (Al, Ca), fayalite (Fe), olivine (Mg), albite (Na), and microcline (K) with basaltic glass VG-2 used as a secondary standard. Errors are generally <2% for major elements and <10% for minor elements.

Raman Spectroscopy

Mineral inclusions were identified using Raman spectroscopy at the Gemological Institute of America (GIA) in Carlsbad, CA collected with a Renishaw inVia Raman microscope system. The Raman spectra of the inclusions were excited by a Stellar-REN Modu Ar-ion laser at 514 nm and collected at a nominal resolution of 3 cm^{-1} in the 2000–200 cm^{-1} range. Each spectrum of the inclusions was accumulated three times for 10 s each at 20× or 50× magnification. Confocal optics allowed inclusions beneath the surface to be analyzed without having to polish through the inclusion and without significant interference from the host corundum.

LA-ICP-MS analysis

LA–ICP–MS sapphire analyses were performed at GIA Carlsbad, CA on a Thermo Scientific iCap-Q ICP–MS with plasma rf power of 1400 W coupled with a New Wave Research UP-213 laser ablation unit with a frequency-quintupled Nd:YAG laser (213 nm wavelength with 4 ns pulse width). A laser spot-size of 55 μm was used with a fluence of 10±1 J/cm^2 and 15 Hz repetition rate. NIST 610 and 612 glasses were used for standardization using ^{27}Al as an internal standard. Isotopes measured are ^{24}Mg, ^{47}Ti, ^{51}V, ^{52}Cr, ^{57}Fe, ^{71}Ga. Additional LA–ICP–MS core and rim analyses were performed on seven blue Yogo sapphires and two reddish-violet Yogo sapphires using a New Wave Excimer laser ablation system at the Queensland University of Technology following a modified procedure from Wong et al. (2017). A laser spot-size of 100 μm was used with a fluence of 2.5 (J/cm^2) and 7 Hz repetition rate. Data were processed using the software package, Iolite (Paton et al. 2011), based on the calculation style of Longerich et al. (1996), using the same reference materials and internal standards as mentioned above. Detection limits are reported in **Table 2** and relative standard deviations are generally <5% for all isotopes.

Oxygen Isotope Measurements

Oxygen isotopic measurements of the same seven blue Yogo sapphires and two reddish-violet Yogo sapphires were carried out with the Sensitive High Resolution Ion Microprobe – Stable Isotopes (SHRIMP-SI) at the Research School of Earth Sciences, Australian National University. Yogo sapphire crystals were mounted in conventional 1-inch epoxy mounts and ground to expose cross sections of the crystals, then polished to 1 micron diamond paste. The polished mounts were cleaned and coated with 30nm of gold, then loaded into a steel holder. SHRIMP-SI measurements were performed with a Cs^+ primary beam of ~ 2 nA, 15 keV, focused to sputter an area of ~ 20 x 30 µm. Negative secondary ions were extracted and accelerated through a total of 10 kV, and $^{16}O^-$ and $^{18}O^-$ were measured simultaneously on Faraday cups. The electrometers measuring $^{16}O^-$ and $^{18}O^-$ were set to 10^{11} Ω (50V range) and 10^{11} Ω (5V range), respectively. Charge neutralization of the sample surface was achieved using a focused oblique-incidence, high energy electron gun. Electrons were delivered to the target surface with an energy of ~ −1.8 keV. Analyses were corrected for isotopically fractionated electron-induced secondary ion emission (Ickert et al., 2008). For the oxygen isotope measurements presented here the collector slit widths were set at 400 µm for $^{16}O^-$ and 300 µm for $^{18}O^-$. Typical count rates on $^{16}O^-$ were ~ $1.6 – 2.0 \times 10^9$ cps, and on $^{18}O^-$ about $3.3 – 4.0 \times 10^6$ cps. Each analysis took about 6 min and consisted of 120 s of presputtering, ~ 100 s of automated steering of secondary ions, ~ 5 s of automated centering of the secondary ions in the collector slits with magnet control, and 120 s of data collection, which consisted of 1 set of 6 scans, 20 s each, with each scan comprising ten 2 s integrations. Isotopic ratios have been corrected for instrumental mass fractionation by applying a correction factor calculated from the analyses of a synthetic corundum reference material with known $^{18}O/^{16}O$ ratio ($\delta^{18}O$ = -6.1 ± 0.3‰). Background counts were subtracted from the total counts (^{16}O and ^{18}O mass positions) prior to ratio calculation. The corrected $^{18}O/^{16}O$ ratios are then expressed in standard $\delta^{18}O$ notation in

144 permil (‰) relative to VSMOW. The internal precision of $\delta^{18}O$ of individual measurements was typically
145 0.1–0.3 ‰ (2SE). The reproducibility of $\delta^{18}O$ was ca. 0.2 ‰ (1SD).

146 Oxygen isotope compositions of the synthetic corundum reference material were measured by
147 laser fluorination (LF) at GNS Science, New Zealand (Analyst: Dr. Jannine Cooper). Oxygen was extracted
148 from sample powders for isotope analyses using a CO_2-laser and BrF_5 (Sharp, 1990). Samples and
149 standards were heated overnight to 150°C prior to loading into the vacuum extraction line. These were
150 then evacuated for approximately 6 hours. Blank BrF_5 runs were done until yield was less than 0.2 moles
151 oxygen. Oxygen yields were recorded and CO_2 gas analysed on a Geo20-20 mass spectrometer. Samples
152 were normalized to the international quartz standard NBS-28 using a value of +9.6 ‰. Values for NBS-28
153 analysed with the samples had values that varied by less than 0.15 ‰. Five analyses gave an average
154 $\delta^{18}O$ value of -6.1 ± 0.3‰ for the synthetic corundum reference material.

155 *Sample Description*

156 Sapphires and rubies analyzed here were from the collections of Nathan Renfro of the
157 Gemological Institute of America and from Will Heierman of Earth's Treasures, or from the Gemological
158 Institute of America's reference collection which was collected in the field by Vincent Pardieu of the
159 Gemological Institute of America. Synthetic ruby standards were purchased from Aussie Sapphire
160 Lapidary Warehouse. All samples analyzed were small (usually <5 mm), gem quality, transparent rubies
161 and sapphires. Samples analyzed in this study include 14 rubies from Pailin, Cambodia, 10 rubies from
162 Chantaburi-Trat, Thailand, and 44 sapphires from Yogo Gulch, Montana, USA. Samples from Yogo Gulch
163 were generally flat, tabular hexagonal prisms while those from Thailand and Cambodia tended to be
164 rounded to angular fragments not showing any crystal faces. Note, the color of the sapphires from Yogo
165 Gulch generally ranged from light, cornflower blue to violet to reddish-violet to (rarely) red. The latter
166 variety ought to bear the moniker "ruby"; however, the color of these samples seems to vary

continuously from blue to violet to red with concomitant continuous variations in chemistry. Given that there are no clear-cut boundaries for the boundary between reddish-violet sapphire and ruby, we have opted to simply not use the term "ruby" for gem corundum from Yogo. Instead, we will refer to (blue) sapphires and reddish-violet sapphires from Yogo. This is a reasonable solution since the color of this gem corundum is not the focus of this manuscript. We generally placed three LA-ICP-MS spots on each sample but some samples had more than three spots. See Supplementary Table S1 for the full analyses.

Results and Discussion:

Trace Element Chemistry

The trace element chemistry measured by LA–ICP–MS analysis is summarized in **Table 1** with full results in **Table S1** in the data depository. Plots of the full analyses are shown in **Figures 1**–**4**. In these plots the Thai and Cambodian rubies were grouped together for simplicity as they have overlapping trace element signatures. These plots show, in general, the broadly similar trace element chemistry of Thai/Cambodian rubies and Yogo sapphires. In summary, Thai rubies have an average of 150 ppm Mg, 148 ppm Ti, 2986 ppm Fe, and 26 ppm Ga, Cambodian rubies have an average of 129 ppm Mg, 136 ppm Ti, 2957 ppm Fe, and 24 ppm Ga, while Yogo sapphires have an average of 128 ppm Mg, 215 ppm Ti, 3219 ppm Fe, and 47 ppm Ga. The concentration of Cr is much more variable than the other trace elements here ranging from 450-7761 ppm in Thai rubies (median = 2410 ppm), 955-2856 ppm in Cambodian rubies (median = 2123 ppm), and 2-12590 ppm in Yogo sapphires (median = 286). However, note that Cr-rich Yogo samples were deliberately oversampled here for the sake of comparison with Thai/Cambodian rubies. **Table 1** also provides several elemental ratios used to separate "magmatic" from "metamorphic" sapphires such as Ga/Mg, Ga*/Al (= 10,000×Ga/Al), Cr/Ga, and Fe/Ti. Overall, the chemistry of gem corundum from these two deposits is largely similar relative to other worldwide gem corundum deposits (e.g. Peucat et al. 2007) with high values of Mg, relatively high Fe, and relatively low

values of Ga. Nonetheless, **Figure 4a**–**b** clearly shows that sapphires and rubies from these deposits can be confidently separated based on their relative concentrations of Mg, Ga, and Ti. The most obvious distinction is the overall higher concentrations of Ga in Yogo sapphires and higher concentrations of Mg relative to Ti in Thai/Cambodian rubies (**Figure 4b**). The latter relationship is important as the co-substitution of Mg^{2+} and Ti^{4+} for two Al^{3+} cations is likely the most important mechanism for incorporation of both Mg and Ti in ruby and sapphire. Both of these relationships are also apparent in **Figures 1–2**.

Figures 1–3 also show trace element data in relation to various discriminant diagrams developed by researchers (Sutherland et al. 1998; Peucat et al. 2007) to differentiate between "magmatic" and "metamorphic" sapphires and rubies. Thai/Cambodian rubies and Yogo sapphires generally show an affinity for the "metamorphic" fields in these diagrams. The main difference in trace element chemistry is in the Cr content (**Figure 3**). This is, of course, related to the fact that only rubies (red Cr-bearing gem corundum) were analyzed from Thailand and Cambodia while a range of colored gem corundum from blue to reddish-violet was analyzed from the Yogo Gulch deposit. This is illustrated most clearly in **Figure 3,** which plots Fe/Ti against Cr/Ga and shows a continuous variation in Cr/Ga values for Yogo sapphires from values close to those of Thai/Cambodian rubies down to very low Cr/Ga values. Note that Yogo sapphires cross over into the "magmatic" domain defined in **Figure 3**. It is frequently assumed that Cr-enrichment in gem corundum is indicative of a metamorphic genesis rather than a magmatic origin. However, the continuous and seamless variation from ostensibly "magmatic" blue to "metamorphic" reddish-violet sapphires from Yogo Gulch suggests that Cr-enrichment is not diagnostic of a metamorphic origin. In fact, the presence of silicate melt inclusions in blue sapphires and reddish-violet sapphires from Yogo and rubies from Thailand and Cambodia suggests that they all ought to be considered as magmatic rubies and sapphires irrespective of their Cr concentrations.

One of the most commonly used trace element discriminants to distinguish between magmatic and metamorphic gem corundum is the overall Ga concentrations and the Ga/Mg ratio. In general, gem corundum with low values of Ga (<100 ppm) and Ga/Mg < 3 are considered to have a "metamorphic" origin and high Ga (>100 ppm) and Ga/Mg > 3 is considered to suggest a "magmatic" origin. The 100×Mg–10×Ti–Fe ternary is also used where higher Mg values indicate a metamorphic origin and higher Fe values a magmatic origin. Nonetheless, the gem corundum studied here is generally classified as "metamorphic" except for a small proportion of analyses plotting in the magmatic field in the Cr/Ga vs. Fe/Ti diagram (**Figure 3**). As proposed above, the silicate melt inclusions in these rubies and sapphires suggest that it is reasonable to consider them to have a magmatic origin. It seems, then, that the problem of differentiating between magmatic and metamorphic sapphires through trace element chemistry ought to be revisited.

Finally, one discriminant plot that is becoming more widely accepted is the $FeO+TiO_2+Ga_2O_3$ vs. $FeO-MgO-V_2O_3-Cr_2O_3$ plot of Giuliani et al. (2015). Thai/Cambodian rubies and Yogo sapphires generally lie in the "ruby in mafic-ultramafics" field in this plot (**Figure 4c**). This is generally consistent with our model considering that basic rocks such as anorthosites are commonly genetically similar to mafic-ultramafics. The usefulness of this discriminant diagram may lie in its classification based on the likely composition of the protolith to the gem corundum and its avoidance of attempting to determine magmatic vs. metamorphic origin from trace elements. Note, however, that many Yogo sapphires and some Thai/Cambodian rubies also lie in the "corundum in metasomatite" field which clearly would not be an accurate classification.

Melt Inclusions

Glassy melt inclusions are found frequently in Thai and Cambodian rubies (Gübelin and Koivula 2008). They are identified by their negative-crystal morphology imposed on the inclusion by the

238 corundum crystal lattice and by the presence of a spherical contraction bubble (**Figure 5a**). Glassy melt
239 inclusions are generally 25–100 μm in size. Also observed are larger light-colored, opaque inclusions that
240 have a negative-crystal morphology defined by the corundum crystal lattice. These inclusions generally
241 range from 200–500 μm in size and have a "sugary" appearance suggesting they are polycrystalline
242 aggregates (**Figure 5b**). The negative-crystal morphology of these larger inclusions suggests that they are
243 also melt inclusions that recrystallized after entrainment in the corundum.

244 Melt inclusions are observed in blue sapphires from Yogo Gulch, MT as reported previously by
245 Palke et al. (2016). Glassy melt inclusions in Yogo sapphires are <50 μm and are generally smaller than in
246 the Thai and Cambodian rubies. Nonetheless, these inclusions are also typified by their negative crystal
247 morphology and contraction bubble (**Figure 5c**). Larger negative-crystal-shaped, light-colored, opaque
248 inclusions are seen in Yogo sapphires as well and are also interpreted to represent recrystallized melt
249 inclusions (**Figure 5d**). Gübelin and Koivula (2008) and Palke et al. (2016) reported the presence of
250 multiphase analcime and calcite inclusions in Yogo sapphires. The inclusions identified by Palke et al.
251 (2016) were negative-crystal shaped, light-colored inclusions that were interpreted to be recrystallized
252 melt inclusions as described above. Palke et al. (2016) further suggested that these larger recrystallized
253 melt inclusions may simply be larger, recrystallized versions of the smaller glassy silicate melt inclusions.
254 However, further consideration of the mineralogical composition of these analcime/calcite melt
255 inclusions suggests that it is unlikely that they have the same bulk composition as the smaller silicate
256 glass inclusions. Palke et al. (2017) suggested that these larger, recrystallized melt inclusions and the
257 smaller glassy melt inclusions actually represent immiscible silicate and carbonatite melts produced
258 during the partial melting event that produced the corundum. Similar bimodal melt inclusion suites have
259 been noted in peritectic garnet produced during partial melting events (Ferrero et al. 2016). The larger
260 recrystallized melt inclusions in Thai/Cambodian rubies may also indicate that rubies crystallized in the

261 presence of immiscible silicate and carbonatite melts during a partial melting event although further
262 work is required to analyze the mineralogy of these inclusions.

263 While the rarity of Cr-rich gem corundum from Yogo Gulch, MT made it difficult to make
264 microscopic observations on a statistically large population of reddish-violet sapphires, one glassy melt
265 inclusion was observed in a deep red Yogo ruby. This sample was prepared for EPMA measurements on
266 the glassy melt inclusion in addition to melt inclusions in one ruby from Thailand and Cambodia each.
267 The results of these analyses are shown in **Table 2** in addition to the results from Palke et al. (2016) for
268 blue sapphires from Yogo Gulch, MT. The melt inclusions in all cases are broadly similar in composition
269 with SiO_2 ranging from 53.4 to 60.5 wt.%, Al_2O_3 from 20.6 to 24.0 wt.%, and are moderately enriched in
270 CaO and Na_2O from 4.9 to 6.2 wt.% and 4.3 to 5.2 wt.%, respectively. In general, melt inclusions have
271 relatively low concentrations of TiO_2 (0.1–0.4 wt.%), MgO and FeO_{tot} (0.4–1.9 wt.% each), and K_2O (0.1–
272 1.7 wt.%), with the exception of the Cambodian ruby with 3.1 wt.% K_2O. The higher CaO content of
273 these melt inclusions makes them distinct from the low-CaO syenitic or phonolitic melt inclusions
274 measured in classical blue-green-yellow basalt-related sapphires (Izokh et al. 2010; Baldwin et al. 2017).
275 Dissolved volatile concentrations can be measured as the difference in oxide totals from 100 wt.%
276 (**Table 2**). For blue Yogo sapphires average volatile content in the melt inclusions are 9.0 wt%, the melt
277 inclusions in the Yogo ruby, Thai ruby, and Cambodian ruby studied here have 6.7, 6.3, and 7.5 wt.%
278 dissolved volatiles, consistently lower than for the Yogo blue sapphires. Overall, the melt inclusions in
279 Yogo sapphires and the preliminary sampling of Yogo, Thai, and Cambodian rubies studied here have
280 broadly similar compositions.

281

282 *Mineral Inclusions*

283 The most common mineral inclusions in Yogo sapphires are plagioclase feldspar, garnet, and
284 blocky to columnar rutile (i.e. not needle-like or “silky” rutile). Less frequently, apatite, phlogopite, and

zircon have been reported (Gübelin and Koivula 2008; Palke et al. 2016). Analcime and/or calcite inclusions are reported in Yogo sapphires; however, as described above these are likely multiphase inclusions that represent recrystallized melt inclusions and are not primary analcime and/or calcite inclusions.

In this study the most commonly observed mineral inclusion in Thai and Cambodian rubies is clinopyroxene with occasional identification of garnet inclusions. Plagioclase feldspar has also been identified as an inclusion in Thai/Cambodian rubies (Sutherland et al. 1998; Hughes et al. 2017); however, the absence of plagioclase inclusions in this study suggests they are less common than clinopyroxene and garnet inclusions. More rarely, but perhaps more importantly for the genetic model that will be outlined below, sapphirine has been reported as an inclusion in Thai rubies (Koivula and Fryer, 1987; Sutthirat et al. 2001; Saminpanya and Sutherland, 2011; Khamloet et al. 2014).

Oxygen isotopes

Previous $\delta^{18}O$ measurements for ruby from Cambodia gave a range of 2.4 to 4.9 ‰ (Giuliani et al. 2005) while Yui et al. (2006) reported $\delta^{18}O$ values of 1.3 to 4.2 ‰ for rubies from Thailand. Furthermore, Giuliani et al. (2005) measured $\delta^{18}O$ values of 5.4 to 6.8 ‰ for Yogo sapphires. Additional oxygen isotope data was collected on a small suite of blue to reddish-violet Yogo sapphires in this study and the results are shown in **Figure 6**. This new data significantly increases the range of $\delta^{18}O$ values for Yogo sapphires to 4.5-7.7 ‰. Note also that the two reddish-violet sapphires analyzed here have a lower range of $\delta^{18}O$ from 4.5 to 5.4 ‰ while the blue to violetish-blue sapphires range from 5.7 to 7.7 ‰. LA-ICP-MS data were also collected on these samples with the ablation pits placed as close as possible to the spots analyzed by SHRIMP for a comparison between trace element and oxygen isotope data. The full results of our oxygen isotope analyses and the additional accompanying LA-ICP-MS data are contained in **Table S2** in the data depository. $\delta^{18}O$ of the Yogo sapphires show a generally negative

correlation with Cr and Mg, and positive correlation with Ga (**Figure 6**). However, note that the sample size analyzed here is relatively small and the nature of the correlation (linear correlation or otherwise) cannot be determined. Core to rim measurements were made on several samples. The sapphires analyzed are generally homogeneous in their oxygen isotope compositions from core to rim which has been noted before in other cases (e.g. Yui, et al. 2003; Sutherland, et al. 2017).

The Genetic Model

Palke et al. (2016) argued that the Na- and Ca-rich melt inclusions in Yogo sapphires suggest corundum formation during partial melting of hydrated and carbonated lower crustal anorthosites or troctolites by local intrusion of the lamprophyre that eventually transported the sapphires to the surface. Anorthite-plagioclase-rich rocks such as anorthosites are likely candidates as they are sufficiently Al-rich to form corundum during partial melting and Ca-rich enough to explain the relatively high CaO concentrations in the glassy melt inclusions. Anorthosites or similar rocks are also reasonable protoliths as they are relatively rare in the Earth (e.g. Ashwal 1993). Given the rarity of sapphire and ruby deposits, it is almost necessary that the rocks producing them are similarly rare. This conclusion rested largely on the similarity between globular, light-color structures (leucocratic ocelli) composed of analcime and calcite in the Yogo lamprophyre and the analcime- and calcite-bearing inclusions in sapphires, which were interpreted to be crystallized melt inclusions. It was argued that the leucocratic ocelli and the melt inclusions had a common origin through partial melting of a precursor, hydrated and carbonated anorthosite (although as argued above these likely represent a carbonatite melt that was immiscible in the silicate melt represented by the smaller glassy melt inclusions). Palke et al. (2016) also modeled this process using the MELTS package and suggested specifically that corundum can grow during such a process through an incongruent melting reaction of another Al-rich mineral such as kyanite.

The similarity in trace element chemistry and melt inclusion compositions for Thai/Cambodian rubies and Yogo sapphires suggests these gem corundum deposits may have been produced through similar geological processes (i.e. corundum formation through partial melting of an anorthosite, although note our discussion of nomenclatural issues for anorthosites below). One argument against this hypothesis is that the inclusion suites in the gem corundum vary between the two deposits. Garnets and melt inclusions occur in both cases but Yogo sapphires commonly have plagioclase and rutile with rare apatite and zircon inclusions while Thai/Cambodian rubies host dominantly clinopyroxene with less common garnet, plagioclase, and sapphirine inclusions. On face value this appears to discredit the hypothesis of a common origin. However, taking a simple approach and considering the melting relations in the forsterite-anorthite-quartz ternary (at 2.0 GPa, Liu and Presnall 1990) suggests a way forward. In this diagram (**Figure 7**) there exists a field for corundum (Co) near the anorthite apex. A super-liquidus melt with its bulk composition in this corundum field will crystallize corundum at the liquidus. However, this corundum will incongruently react with the liquid upon further cooling to crystallize anorthite. Note that in this system corundum will not persist as a sub-solidus mineral in the case of equilibrium crystallization. Alternatively, if we start to melt a solid rock with the same bulk composition in this corundum field, we would see corundum start to crystallize through an incongruent melting reaction once the liquid reached the corundum field.

We can illustrate how one might produce two different inclusion suites by slightly altering the bulk composition. We take two different hypothetical protoliths with overall similar bulk compositions lying in the corundum field of the An-Fo-Qz ternary at 2.0 GPa (**Figure 7**), but with one being more enriched in a forsterite component and the other being more enriched in a quartz component (i.e. one more mafic and one more felsic). Note that both compositions roughly represent an anorthosite protolith. The more felsic anorthosite was chosen to be composed of dominantly anorthite and equal components of quartz and enstatite at subsolidus conditions. The first melt occurs at point E which also

has nearly equal amounts of an enstatite and quartz component. Therefore, after the melting has consumed all the enstatite and quartz, the liquid will leave point E on a projection toward the anorthite apex (blue path, **Figure 7**). Once the liquid reaches the boundary between anorthite and corundum, the leftover anorthite will melt incongruently to produce corundum. If the corundum produced in this way could be preserved, the dominant mineral inclusion in corundum would be anorthite. The more mafic protolith was chosen to be composed of dominantly anorthite with minor enstatite and only a small amount of quartz at subsolidus conditions. In this case, the first liquid is also at E but quartz will be consumed quickly and the liquid will evolve along the enstatite-anorthite join (red path, **Figure 7**). When the liquid meets the anorthite-enstatite-sapphirine point, sapphirine will crystallize. At this point enstatite will fully melt and the liquid will evolve along the sapphirine-anorthite join. As in the case above, once the liquid reaches the boundary with corundum, anorthite will melt incongruently to produce corundum. In this scenario, coexisting sapphirine could become included in the resulting corundum in addition to anorthite. In fact, a recent study by Karmakar et al. (2017) provides some petrological evidence that this is a plausible scenario. In that study, Karmakar et al. (2017) interpreted corundum coexisting with sapphirine to have been formed during incongruent melting of a hydrated anorthosite.

Obviously this simplified three component model cannot fully explain all of the observations for gem corundum from these deposits. For one thing, the relatively Na_2O-enriched melt inclusions suggest that Na_2O was likely an important component in sapphire and ruby genesis. Additionally, the presence of clinopyroxene and garnet inclusions is obviously not accounted for in the simple forsterite-anorthite-quartz ternary. Furthermore, the volatile-enriched melt inclusions also suggest that H_2O and/or CO_2 were essential components in the processes that formed sapphire and ruby and their involvement will undoubtedly alter the phase diagram shown in the An-Fo-Qz ternary in **Figure 7**. Nonetheless, this simple system can qualitatively show how significantly different inclusion suites in gem corundum might

be generated through the same geological process (partial melting of an anorthosite) due only to relatively small differences in bulk composition.

In fact, this model may also help explain differences in trace element chemistry between these two deposits. For instance, it could be argued that a more mafic protolith should have been involved in Thailand and Cambodia in order to supply Cr for the rubies produced there. The relatively rare occurrence of ruby and violet sapphires in Yogo Gulch, then, suggests that the protolith there was predominantly more felsic but perhaps with some more mafic enclaves that locally supplied Cr to the gem corundum. A more mafic protolith for the reddish-violet sapphires from Yogo is also supported by their lower $\delta^{18}O$ (from 4.5 to 5.4 ‰). The overall lower Ga content of rubies from Thailand and Cambodia also suggests a more mafic protolith as Shaw (1957) has shown that ratios of Ga*/Al (= 10,000×Ga/Al) are lower for "basic igneous" rocks (0.6–1.7) than for "granitic and alkalic" igneous rocks (0.9–4.5). Finally, the higher average concentration of Mg in Thai/Cambodian rubies is also consistent with the involvement of a more mafic protolith. Notably, trace element vs. oxygen isotope ratio patterns also corroborate this narrative with higher Mg and Cr and lower Ga evidently correlated with the lower $\delta^{18}O$ in **Figures 6b–d**.

One problem with this model is the lower frequency of plagioclase inclusions in rubies from Thailand and Cambodia than for Yogo sapphires. If Thai/Cambodian rubies were derived from the partial melting of an anorthosite (i.e. a plagioclase-dominant igneous rock) one would expect to find plagioclase as a common inclusion. One possible explanation may be that the Thai and Cambodian rubies originated at higher pressures deeper within the Earth. In this case, it may be possible that Thai and Cambodian rubies originated from partially melting a rock that was initially an anorthosite, but which was subducted and buried deep within the Earth to pressures at which plagioclase feldspar was less stable and largely replaced by other phases such as clinopyroxene and garnet. In fact, Kornprobst et al. (1990), Morishita et al. (2001), and Gysi et al. (2011) have described corundum-bearing garnet clinopyroxenites in

peridotite bodies and have interpreted these to represent original plagioclase-rich gabbros that were subsequently buried and converted to garnet clinopyroxenites at high pressures. Note that in all cases sapphirine was found as a minor constituent as well (although not necessarily in direct contact with corundum). Additionally, Raheim and Green (1974) used experimental petrology to show that an originally gabbroic anorthosite protolith corresponding to some lunar highland basalts could be converted to an assemblage of garnet + clinopyroxene + kyanite + quartz at high pressures of around 2.0 GPa. Raheim and Green (1974) also showed that in this system corundum would be produced as a supersolidus phase from this assemblage through an incongruent melting reaction but would not exist below the solidus. It is likely, then, that the Thai and Cambodian rubies were derived from a high-pressure clinopyroxenite that was, in turn, derived from a similar (but possibly more mafic) anorthositic protolith as sapphires from Yogo Gulch. In our model, we suggest that the protolith involved in sapphire and/or ruby formation was initially an anorthosite emplaced near the base of the continental crust during ancient (Yogo, Palke et al. 2016) or more modern subduction events (Thailand/Cambodia). In this case, a higher pressure of formation for Thai and Cambodian rubies agrees well with estimates of crustal thickness in the region of the ruby mines in Thailand (50–60 km, Promprated et al. 2003) compared to estimates for crustal thickness in central Montana (around 40 km, Mahan et al. 2012; Purevsuren 2014).

A note on nomenclature

We suggested above an origin for Yogo sapphires and Thai/Cambodian rubies from partial melting of anorthosites. Strictly speaking, using the accepted nomenclature of Streckeisen (1976), anorthosites are igneous rocks composed of >90 % plagioclase. Other plagioclase-rich plutonic rocks include leucotroctolites and leucogabbros (>65 % plagioclase with the remainder as mafic minerals). Ashwal (1993) further subdivided leucogabbros and leucotroctolites into varieties with >77.5 % plagioclase being labelled “gabbroic anorthosites” and “troctolitic anorthosites” and from 65-77.5 %

429 plagioclase as “anorthositic gabbros” and “anorthositic troctolites”. Note that the hypothetical
430 protoliths from **Figure 7** would not strictly be considered as “anorthosites” but rather gabbroic or
431 troctolitic anorthosites according to Ashwal (1993). However, as a matter of convenience and clarity, the
432 term “anorthosite” is used somewhat loosely here to denote plagioclase-dominant rocks including
433 gabbroic or troctolitic anorthosites and possibly even anorthositic troctolites or gabbros.
434
435 *What do the oxygen isotope data say?*
436 Palke et al. (2016) noted that the range in $\delta^{18}O$ values for Yogo sapphires (new data here
437 extends it to 4.5 to 7.7 ‰) is within the range given by Kempton and Harmon (1992) of 5.4 to 13.5 ‰ for
438 lower crustal xenoliths. Similarly, $\delta^{18}O$ values for plagioclase from mantle-related anorthosites range
439 from 5.8 to 7.6 ‰ or 7.7 to 12.1 ‰ (Taylor 1968) for plagioclase from Proterozoic anorthosites from
440 Quebec which are assumed to have involved some degree of crustal assimilation (Peck and Valley 2000).
441 These ranges seem to be at odds with the lower range of $\delta^{18}O$ values from 1.3 to 4.9 ‰ for
442 Thai/Cambodian rubies. However, it should be noted that little is actually known about oxygen isotope
443 fractionation factors between corundum and a silicate melt or other buffering fluids/minerals. Assuming
444 an anorthositic protolith was involved in the formation of Thai/Cambodian rubies but that it was
445 metamorphosed into a clinopyroxenite, as a first approximation we can use the calculated mineral-
446 water fractionation factors of Zheng (1991) and Zheng (1993) to derive a fractionation of 4.2 ‰
447 between diopside and corundum at 850 °C with corundum being isotopically lighter [temperature of 850
448 °C chosen to correspond to formation conditions as suggested by Palke et al. (2016)]. In this case, even
449 the very lowest $\delta^{18}O$ value of 1.3 ‰ for Thai ruby would be in equilibrium with diopside with $\delta^{18}O$ of 5.5
450 ‰, which is right at the lower range for lower crustal xenoliths given by Kempton and Harmon (1992)
451 and anorthosites from Taylor (1968). It should be noted, however, that clinopyroxene from a high-
452 pressure metamorphosed anorthosite is likely to be quite Al-rich involving a significant Ca-Tschermak

453 (CaTS) component ($CaAl_2SiO_6$) and so the use of a fractionation factor between diopside and corundum
454 is a very rough approximation.
455
456
457 **Implications:**
458
459 *Gem corundum as xenocrysts but not "accidental" xenocrysts*
460 One of the more important conclusions from this work is that these sapphires and rubies are
461 considered xenocrysts in their volcanic hosts, but they are not "accidental" xenocrysts as their formation
462 is directly related to the interaction between the transporting mafic magmas and Al-rich (but corundum
463 free) lower crustal protoliths. If the sapphires and rubies were, in fact, "accidentally" entrained, this
464 would require a significant portion of the Earth's lower crust or upper mantle to be corundum-bearing in
465 areas hosting large basalt-related sapphire and ruby deposits (e.g. eastern Australia and southeast Asia).
466 On the other hand, in the partial melting model, the preexistence of corundum is not necessary as
467 basalts can generate corundum by partially melting Al-rich rocks as they pass through the lithosphere.
468 This model suggests that not all xenocrysts necessarily represent faithful records of the formations that
469 magmas pass through on their journey to the Earth's surface. In fact, it is known that other
470 peraluminous minerals such as garnet also often grow *during* incongruent melting reactions when
471 crustal rocks are partially melted (Cesare et al. 2011). Given the close association between gem
472 corundum deposits and hot, mantle-derived volcanics, this partial melting model is intuitively appealing
473 and ought to be considered as a possible origin of other volcanically-associated sapphire and ruby
474 deposits, even those that are obviously distinct from the Yogo and Thai/Cambodian gem corundum (e.g.
475 the eastern Australian blue-green-yellow [BGY] suite of alkali basalt-related sapphires).
476

Comparison to eastern Australian rubies

For eastern Australian alluvial sapphires and rubies, the distinction of 'magmatic' and 'metamorphic' sources through trace elemental ratios have already been questioned, due to the finding of a continuous spectrum of trace elemental compositions by Wong et al. (2017). Eastern Australian sapphires are generally associated with a 'magmatic' origin, whereas rubies have been associated with a 'metamorphic' source. Similarities between Thai/Cambodian rubies and eastern Australian rubies suggest that Australian alkali basalt-related rubies may have been formed by magmatic processes as well. The occurrence of Al-rich diopside and sapphirine mineral inclusions in eastern Australian rubies are similar to those observed in Thai/Cambodian rubies. Rubies found from the Cudgegong-Macquarie River system in New South Wales also contain high-Al clinopyroxene inclusions (Sutherland et al. 2003) similar to the Thai/Cambodian rubies and may also fit into the anorthosite partial melting model. Additionally, feldspathic melt inclusions are found in Australian pink to lavender sapphires from Barrington Tops (Zaw et al. 2006) suggesting a magmatic origin. Trace element chemistry of pink sapphires and rubies from Table 2 of Zaw et al. (2006) shows them to be very similar to the Thai/Cambodian rubies and Yogo sapphires and rubies studied here (averages for Barrington corundum: Ti = 140 ppm, Fe = 4292 ppm, Cr = 744 ppm, V = 51 ppm, Ga = 30 ppm; Zaw et al. 2006), suggesting a similar origin as well. Furthermore, Sutherland and Coenraads (1996) described an alkali basalt related ruby-sapphire-sapphirine-spinel xenolith from the Barrington volcanic province in New South Wales, Australia. Sapphirine-spinel thermometry suggested a temperature of formation from 780–940 °C for this assemblage, similar to temperature estimates for formation of the Yogo sapphires and in line with an origin through low-degree partial melting. The results of Sutherland and Coenraads (1996) show that sapphirine-ruby assemblages can be consistent with temperatures that are likely to be near-solidus and are, hence, consistent with a partial melting scenario.

Of particular note is the range in oxygen isotope composition of eastern Australian rubies, 3.6 to 5.9‰ (Giuliani et al. 2005; Zaw et al. 2006; Graham et al. 2008; Sutherland et al. 2009, 2017), which is transitional between those observed in the reddish-violet Yogo sapphires from this study (4.5 to 5.4‰) and Thai/Cambodian rubies (1.3 to 4.9‰). This transition in oxygen isotope compositions shows that basalt-related rubies appear to have a continuous spectrum of $\delta^{18}O$ values. While we suggest that Cr-rich gem corundum from these deposits may have a common origin, as argued above, variations in the range of $\delta^{18}O$ values for a specific deposit may be related to variations in the extent of the "mafic" character of the protolith with more mafic compositions producing corundum with lower $\delta^{18}O$ value. Note that Yogo sapphires and eastern Australian sapphires extend this continuous spectrum of $\delta^{18}O$ values further (5.5 to 7.7‰ and 4.6 to 6.5‰ respectively), suggesting that more felsic compositions having higher $\delta^{18}O$ values. However, further work on rubies from other deposits is warranted to support this hypothesis. Specifically, further analysis of mineral and melt inclusions in eastern Australian rubies could support this claim.

Can trace elements separate magmatic and metamorphic gem corundum?

The rubies and sapphires studied here add to the list of gem corundum with questionable predictions for geological origin (metamorphic or magmatic) based on trace element chemistry (Izokh et al. 2010; Uher et al. 2012; Sutherland et al. 2015, 2017; Palke et al. 2016, 2017; Baldwin et al. 2017; Wong et al. 2017). The reason for this discrepancy is likely because the original discriminant diagrams were produced with groups of sapphires and rubies that were too narrow to completely represent the full suite of metamorphic and magmatic gem corundum. For instance, while Peucat et al. (2007) reported trace element data for Yogo sapphires, they did not consider them to be magmatic sapphires. If Yogo sapphires had been classified as magmatic at the time, their discriminant diagrams would have looked very different. The same can be said for the alluvial Montana sapphire deposits which significantly overlap both metamorphic and magmatic fields from Peucat et al. (2007) but which have

524 melt inclusions and should be classified as magmatic. It was previously thought that only the blue-green-
525 yellow (BGY) suite of sapphires from alkali basalts were magmatic, but it is clear now that the magmatic
526 group of sapphires needs to be expanded. As it stands, it seems that none of the existing trace element
527 defined discriminant diagrams can accurately separate magmatic and metamorphic sapphires and rubies
528 and it is suggested that these discriminant schemes are used with great caution, if at all.

529 Finally, several previous studies have identified bimodal or polymodal assemblages of
530 magmatic/metamorphic/metasomatic gem corundum in many basalt-related gem fields (i.e. Sutherland
531 et al. 2002, 2008; Yui et al. 2006; Zaw et al. 2006; Peucat et al. 2007; Graham et al. 2008; Saminpanya
532 and Sutherland 2011). These assignments are generally based on trace element chemistry and mineral
533 inclusions. However, given the discussion above, the criteria generally used to discriminate magmatic
534 and metamorphic gem corundum are not robust enough to produce reliable genetic separations. In fact,
535 the observations described show that the mineralogical and chemical properties of so-called
536 "metamorphic" volcanically-associated sapphires and rubies can also be consistent with a magmatic
537 origin. This leaves open the possibility that volcanically-associated "metamorphic" gem corundum from
538 other deposits may, in fact, be magmatic. Taken a step further, this calls into question the suitability of
539 the bimodal (metamorphic/magmatic) or polymodal (metamorphic/magmatic/metasomatic) genetic
540 hypothesis of volcanically-associated gem corundum deposits in general. It may be that all volcanically-
541 associated gem corundum is magmatic and their variations in trace element chemistry, oxygen isotopes,
542 and inclusions are simply caused by differences in the protolith from which the rubies and sapphires
543 were derived.

544

545

546 **Acknowledgements:**

Many thanks go to Dr. Jannine Cooper from GNS, New Zealand for analyzing the corundum standards by laser-fluorination. The authors thank Charlotte Allen from QUT for her help with LA-ICP-MS analyses. We are grateful to Chi Ma of Caltech for his help with EPMA measurements. This work was initiated while one author (AP) was a R.T. Liddicoat Postdoctoral Research Associate at the Gemological Institute of America (GIA) and many thanks are owed to GIA for their support. Thanks also go to Will Heierman of the Corunduminium.com for providing samples for this study and for helpful discussions about Montana sapphires. We appreciate Richard Hughes of Lotus Gemology and John Koivula, Nathan Renfro, and Mike Breeding of the Gemological Institute of America as well for sharing their knowledge of Southeast Asian and American gem corundum deposits. We also thank Ian Graham and Lisa Baldwin for their constructive reviews and Associate Editor Aaron Celestian, Managing Editor Rachel Russell, and the rest of the editorial staff at American Mineralogist for handling and improving this manuscript.

References Cited:

Ashwal, L.D. (1993) Anorthosites. Springer-Verlag, Berlin Heidelberg, Germany.

Baldwin, L.C., Tomaschek, F., Ballhaus, C., Gerdes, A., Fonseca, R.O.C., Wirth, R., Geisler, T., and Nagel, T. (2017) Petrogenesis of alkaline basalt-hosted sapphire megacrysts. Petrological and geochemical investigations of in situ sapphire occurrences from the Siebengebirge Volcanic Field, Germany. Contributions to Mineralogy and Petrology,172, 43

Barr, S.M., and Macdonald, A.S. (1981) Geochemistry and geochronology of Late Cenozoic basalts of Southeast Asia. Geological Society of America Bulletin, 92, 1069-1142. Carlson, W.D. and Lindsley, D.H. (1988) Thermochemistry of pyroxenes on the join $Mg_2Si_2O_6$-$CaMgSi_2O_6$. American Mineralogist, 73, 242-252.

569 Cesare, B., Acosta-Vigil, A., Ferrero, S., and Bartoli, O. (2011) Melt inclusions in migmatites and
570 granulites. Journal of the Virtual Explorer, 38, paper 2.

571 Ferrero, S., Wunder, B., Ziemann, M.A., Wälle, M., and O'Brien, P.J. (2016) Carbonatitic and granitic
572 melts produced under conditions of primary immiscibility during anatexis in the lower crust.
573 Earth and Planetary Science Letters, 454, 121-131.

574 Gaillou, E. (2003) Les saphirs du Massif Central: Etude minéralogique des saphirs du Sioulot, du Mont
575 Coupet et du Menoyre. Détermination de leur origine, 45 p. Master's Thesis, Université Blaise
576 Pascal.

577 Gauthier, G. (1995) Mineralogy, geochemistry, and geochronology of the Yogo dike sapphire deposit,
578 Montana, 289 p. Master's Thesis, University of British Columbia.

579 Giuliani, G., Fallick, A.E., Garnier, V., France-Lanord, C., Ohnenstetter, D., and Schwarz, D. (2005) Oxygen
580 isotope composition as a tracer for the origins of rubies and sapphires. Geology, 33, 249-252.
581 http://dx.doi.org/10.1130/G21261.1.

582 Giuliani, G., Ohnenstetter, D., Fallick, A. E., Groat, L. A., and Fagan, A. J. (2014) The Geology and Genesis
583 of Gem Corundum Deposits, in L.A. Groat, Ed., Geology of Gem Deposits, p. 29-112. Canada,
584 Mineralogical Association of Canada (MAC).

585 Giuliani, G., Pivin, M., Fallick, A.E., Ohnenstetter, D., Song, Y., and Demaiffe (2015) Geochemical and
586 oxygen isotope signatures of mantle corundum megacrysts from Mbujui-Mayi kimberlite,
587 Democratic Republic of Congo, and the Changle alkali basalt, China. Comptes Rendus
588 Geoscience 347, 24-34.

589 Graham, I.T., Sutherland, F.L., Zaw, K., Nechaev, V.P., and Khanchuk, A.I. (2008) Advances in our
590 understanding of the gemcorundum deposits of theWest Pacific continental margins intraplate
591 basaltic fields. Ore Geology Reviews, 34, 200–215.

592 Griffin, W. L., and O'Reilly, S. Y. (1986) The lower crust in eastern Australia: xenolith evidence. Geological
593 Society, London, Special Publications, 24, 363-374.

594 Gübelin, E.J., and Koivula, J.I. (2008) Photoatlas of Inclusions in Gemstones, v.3., 672 p., Opinio
595 Publishers, Basel, Switzerland.

596 Gysi, A.P., Jagoutz, O., Schmidt, M.W., and Targuisti, K. (2011) Petrogenesis of pyroxenites and melt
597 infiltrations in the ultramafic complex of Beni Bousera, northern Morocco. Journal of Petrology,
598 52, 1679-1735.

599 Hollis, J. (1981) Ultramafic and gabbroic nodules from the Bullenmerri and Gnotuk maars, Camperdown,
600 Victoria. Proceedings of the Royal Society of Victoria, 92, 155-167.

601 Hughes, R.W. (2014) Ruby & Sapphire: A Collector's Guide. Lotus Gemology Publishing, Bangkok,
602 Thailand.

603 Hughes, R.W., Manorotkul, W., and Hughes, E.B., (2017) Ruby & Sapphire: A Gemologist's Guide. Lotus
604 Gemology Publishing, Bangkok, Thailand.

605 Ickert, R. B., Hiess, J., Williams, I. S., Holden, P., Ireland, T. R., Lanc, P., Schram, N., Foster, J. J., and
606 Clement, S. W. (2008) Determining high precision, in situ, oxygen isotope ratios with a SHRIMP
607 II: Analyses of MPI-DING silicate-glass reference materials and zircon from contrasting granites.
608 Chemical Geology, 257, 114-128.

609 Izokh, A. E., Smirnov, S. Z., Egorova, V. V., Anh, T. T., Kovyazin, S. V., Phuong, N. T., and Kalinina, V. V.
610 (2010) The conditions of formation of sapphire and zircon in the areas of alkali-basaltoid
611 volcanism in Central Vietnam. Russian Geology and Geophysics, 51, 719-733.

612 Karmakar, S., Mukherjee, S., Sanyal, S., and Sengupta, P. (2017) Origin of peraluminous minerals
613 (corundum, spinel, and sapphirine) in a highly calcic anorthosite from the Sittampundi Layered
614 Complex, Tamil Nadu, India. Contributions to Mineralogy and Petrology, 172, 67.

615 Kempton, P.D. and Harmon, R.S. (1992) Oxygen isotope evidence for large-scale hybridization of the
616 lower continental crust during magmatic underplating. Geochimica et Cosmochimica Acta, 56,
617 971-986.

618 Khamloet, P., Pisutha-Arnond, V., and Sutthirat, C. (2014) Mineral inclusions in sapphire from the basalt-
619 related deposit in Bo Phloi, Kanchanaburi, western Thailand: Indication of their genesis. Russian
620 Geology and Geophysics, 55, 1087-1102.

621 Khanchuk, A., Zalishchak, B., Pakhomova. V., Odarichenko, E., and Sapin, V., (2003) Genesis and
622 gemology of sapphires from the Nezametnoye deposit, Primorye region, Russia. Australian
623 Gemmologist, 21, 329-335

624 King, E.M., Valley, J.W., Davis, D.W., and Kowallis, B.J. (2001) Empirical determination of oxygen isotope
625 fractionation factors for titanite with respect to zircon and quartz. Geochimica et Cosmochimica
626 Acta, 65, 3165-3175.

627 Koivula, J. I., and C. W. Fryer (1987) Sapphirine (not sapphire) in a ruby from Bo Rai, Thailand. Journal of
628 Gemmology, 20, 70.

629 Kornprobst, J., Piboule, M., Roden, M., and Tabit, A. (1990) Corundum-bearing garnet clinopyroxenites
630 at Beni Bousera (Morocco): Original plagioclase-rich gabbros recrystallized at depth within the
631 mantle? Journal of Petrology, 31, 717-745.

632 Limtrakun, P., Zaw, K., Ryan, C. G., and Mernagh, T. P. (2001) Formation of the Denchai gem sapphires,
633 northern Thailand: Evidence from mineral chemistry and fluid/melt inclusion characteristics.
634 Mineralogical Magazine, 65, 725-735.

635 Liu, T.-C., and Presnall, D.C. (1990) Liquidus phase relationships on the join anorthite-forsterite-quartz at
636 20 kbar with applications to basalt petrogenesis and igneous sapphirine. Contributions to
637 Mineralogy and Petrology, 104, 735-742.

638 Longerich, H. P., Jackson, S. E., and Gunther, D. (1996) Laser ablation inductively coupled plasma mass
639 spectrometric transient signal data acquisition and analyte concentration calculation: Journal of
640 Analytical Atomic Spectrometry, 11, 899-904.

641 Mahan, K.H., Schulte-Pelkum, V., Blackburn, T.J., Bowring, S.A., and Dudas, F.O. (2012) Seismic structure
642 and lithospheric rheology from deep crustal xenoliths, Central Montana, USA. Geochemistry,
643 Geophysics, Geosystems, 12.

644 Morishita, T., Arai, S., and Gervilla, F. (2001) High-pressure aluminous mafic rocks from the Ronda
645 peridotite massif, southern Spain: Significance of sapphirine- and corundum-bearing mineral
646 assemblages. Lithos, 57, 143-161.

647 Palke, A.C., Renfro, N.D., and Berg, R.B. (2016) Origin of sapphires from a lamprophyre dike at Yogo
648 Gulch, Montana, USA: Clues from their melt inclusions. Lithos, 260, 339-344.

649 Palke, A. C., Renfro, N. D., & Berg, R. B. (2017) Melt inclusions in alluvial sapphires from Montana, USA:
650 Formation of sapphires as a restitic component of lower crustal melting? Lithos, 278, 43-53.

651 Paton, C., Hellstrom, J., Paul, B., Woodhead, J., and Hergt, J. (2011) Iolite: Freeware for the visualisation
652 and processing of mass spectrometric data. Journal of Analytical Atomic Spectrometry, 26,
653 2508-2518.

654 Peck, W.H., and Valley, J.W. (2000) Large crustal input to high $\delta^{18}O$ anorthosite massifs of the southern
655 Grenville Province: New evidence from the Morin Complex, Quebec. Contributions to
656 Mineralogy and Petrology, 139, 402-417.

657 Peucat, J.E., Raffault, P., Fritsch, E., Bouhnik-Le Coz, M., Simonet, C., and Lasnier, B. (2007) Ga/Mg ratio
658 as a new geochemical tool to differentiate magmatic from metamorphic blue sapphires. Lithos,
659 98, 261-274.

660 Promprated, P., Taylor, L.A., and Neal, C.R. (2003) Petrochemistry of mafic granulite xenoliths from the
661 Chantaburi basaltic field: Implications or the nature of the lower crust beneath Thailand.
662 International Geology Review, 45, 383-406.

663 Purevsuren, U. (2014) Crustal thickness and Vp/Vs beneath the western United States: Constraints from
664 stacking of receiver functions, 103 p. Ph.D. Thesis. Missouri University of Science and
665 Technology.

666 Raheim, A., and Green, D.H. (1974) Experimental petrology of lunar highland basalt composition and
667 applications to models for the lunar interior. Journal of Geology, 82, 607-622.

668 Saminpanya, S. and Sutherland, F.L. (2011) Different origins of Thai area sapphire and ruby, derived from
669 mineral inclusions and co-existing minerals. European Journal of Mineralogy, 23, 683-694.

670 Sharp, Z. D. (1990) Laser-based microanalytical method for the in situ determination of oxygen isotope
671 ratios of silicates and oxides. Geochimica et Cosmochimica Acta, 54, 1353-1357.or

672 Shaw, D.M (1957) The geochemistry of gallium, indium, thallium—a review. Physics and Chemistry of
673 the Earth, 2, 164-211. http://dx.doi.org/10.1016/0079-1946(57)90009-5

674 Streckeisen, A. (1976) Classification and nomenclature of plutonic rocks. Geologische Rundschau, 63,
675 773-786.

676 Sutherland, F.L., and Coenraads, R.R. (1996) An unusual ruby-sapphire-sapphirine-spinel assemblage
677 from the Tertiary Barrington volcanic province, New South Wales, Australia. Mineralogical
678 Magazine, 60, 623-638.

679 Sutherland, F. L., Schwarz, D., Jobbins, E. A., Coenraads, R. R., and Webb, G. (1998) Distinctive gem
680 corundum suites from discrete basalt fields; a comparative study of Barrington, Australia, and
681 West Pailin, Cambodia, gemfields. Journal of Gemmology, 26, 65-85.

682 Sutherland, F.L., Graham, I.T., Pogson, R.E., Schwarz, D., Webb, G.B., Coenraads, R.R., Fanning, C.M.,
683 Hollis, J.D., and Allen, T.C. (2002) The Tumbarumba Basaltic Gem Field, New South Wales: In
684 Relation to Sapphire-Ruby Deposits of Eastern Australia. Records of the Australian Museum, 54,
685 215-248.

686 Sutherland, F.L., Coenraads, R.R., Schwarz, D., Raynor, L.R., Barron, B.J., and Webb, G.B. (2003) Al-rich
687 diopside in alluvial ruby and corundum-bearing xenoliths, Australian and SE Asian basalt fields.
688 Mineralogical Magazine, 67, 717-732.

689 Sutherland, F.L., Giuliani, G., Fallick, A.E., Garland, M., and Webb, G. (2008) Sapphire-ruby
690 characteristics, west Pailin, Cambodia: Clues to their origin based on trace element and O
691 isotope analysis. The Australian Gemmologist, 23, 329-368.

692 Sutherland, F. L., Zaw, K., Meffre, S., Giuliani, G., Fallick, A. E., Graham, I. T., and Webb, G. B. (2009)
693 Gem-corundum megacrysts from east Australian basalt fields: Trace elements, oxygen isotopes
694 and origins: Australian Journal of Earth Sciences, 56, 1003-1022.

695 Sutthirat, C., Charusiri, P., Farrar, E., and Clark, A.H. (1994) New 40Ar/39Ar geochronology and
696 characteristics of some Cenozoic basalts in Thailand. Proceedings of the International
697 Symposium: Stratigraphic Correlation of Southeast Asia, Bangkok, Thailand.

698 Sutherland, F.L., Coenraads, R.R., Abduriyim, A., Meffre, S., Hoskin, P.W.O., Giuliani, G., Beattie, R.,
699 Wuhrer, R., and Sutherland, G.B. (2015) Corundum (sapphire) and zircon relationships, Lava
700 Plains gem fields, NE Australia: Integrated mineralogy, age determination, genesis and
701 geographic typing. Mineralogical Magazine 79, 545-581.

702 Sutherland, F.L., Graham, I.T., Harris, S.J., Coldham, T., Powell, W., Belousova, E.A., and Martin, L. (2017)
703 Unusual ruby-sapphire transition in alluvial megacrysts, Cenozoic basaltic gem field, New
704 England, New South Wales, Australia. Lithos, 278-281, 347-360.Sutthirat, C., Saminpanya, S.,
705 Droop, G.T.R., Henderson, C.M.B., and Manning, D.A.C. (2001) Clinopyroxene-corundum
706 assemblages from alkali basalt and alluvium, eastern Thailand: Constraints on the origin of Thai
707 rubies. Mineralogical Magazine, 65, 277-295.

708 Taylor, H.P., Jr. (1968) The oxygen isotope geochemistry of igneous rocks. Contributions to Mineralogy
709 and Petrology, 19, 1-71.

710 Uher, P., Giuliani, G., Szakáll, S., Fallick, A., Strunga, V., Vaculovič, T., Ozdín, D., and Gregáňová, M.
711 (2012) Sapphires related to alkali basalts from the Cerová Highlands, Western Carpathians (southern
712 Slovakia): Composition and origin. Geologica Carpathica, 63, 71-82.

713 Wass, S. Y., and Hollis, J. (1983) Crustal growth in south-eastern Australia—evidence from lower crustal
714 eclogitic and granulitic xenoliths: Journal of Metamorphic Geology, 1, 25-45.

715 Wilkinson, J. F. G., and Kalocsai, G. I. Z. (1974) Garnet clinopyroxenite inclusions from diatremes in the
716 Gloucester area, New South Wales, Australia: Contributions to Mineralogy and Petrology, 46,
717 275-299.

718 Wilkinson, J. F. G., and Stolz, A. J. (1997) Subcalcic clinopyroxenites and associated ultramafic xenoliths
719 in alkali basalt near Glen Innes, northeastern New South Wales, Australia: Contributions to
720 Mineralogy and Petrology, 127, 272-290.

721 Wong, J., Verdel, C., and Allen, C.M., (2017) Trace-element compositions of sapphire and ruby from the
722 eastern Australian gemstone belt, Mineralogical Magazine, (in press).
723 https://doi.org/10.1180/minmag.2017.081.012

724 Wood, B.J. (1979) Activity-composition relationships in $Ca(Mg,Fe)Si_2O_6$-$CaAl_2SiO_6$ clinopyroxene solid
725 solutions. American Journal of Science, 279, 854-875.

726 Yui, T.-F., Zaw, K., and Limtrakun, P. (2003) Oxygen isotope composition of the Denchai sapphire,
727 Thailand: a clue to its enigmatic origin. Lithos, 67, 153-161.

728 Yui, T.-F., Wu, C.-M., Limtrakun, P., Sricharn, W., and Boonsoong, A. (2006) Oxygen isotope studies on
729 placer sapphire and ruby in the Chanthaburi-Trat alkali basaltic gemfield, Thailand. Lithos, 86,
730 197-211.

731 Zaw, K., Sutherland, F.L., Dellapasqua, F., Ryan, C.G., Yui, T.-F., Mernagh, T.P., and Duncan, D. (2006)
732 Contrasts in gem corundum characteristics, eastern Australian basaltic fields: Trace elements,
733 fluid/melt inclusions and oxygen isotopes. Mineralogical Magazine, 70, 669-687.

734 Zheng, Y.-F. (1991) Calculation of oxygen isotope fractionation in metal oxides. Geochimica et
735 Cosmochimica Acta, 55, 2299-2307.

736 Zheng, Y.-F. (1993) Calculation of oxygen isotope fractionation in anhydrous silicate minerals,
737 Geochimica et Cosmochimica Acta, 57, 1079-1091.

738

739 **Figure Captions:**

740 **Figure 1:** Trace element chemistry of Yogo sapphires and Thai/Cambodian rubies plotting Ga/Mg against
741 Fe. The "metamorphic" and "magmatic" discriminant fields are taken from Peucat et al. (2007)

742 **Figure 2:** Trace element chemistry of Yogo sapphires and Thai/Cambodian rubies in the Mg×100-Ti×10-
743 Fe ternary. The "metamorphic" and "magmatic" discriminant fields are taken from Peucat et al. (2007)

744 **Figure 3:** Trace element chemistry of Yogo sapphires and Thai/Cambodian rubies plotting Cr/Ga against
745 Fe/Ti. The "metamorphic" and "magmatic" discriminant fields are taken from Sutherland et al. (1998)

746 **Figure 4:** Trace element chemistry of Yogo sapphires and Thai/Cambodian rubies plotting **(a)** Ga against
747 Mg and **(b)** Ti against Mg and **(c)** the FeO-MgO-V_2O_3 vs. FeO+TiO_2+Ga_2O_3 plot of Giuliani et al. (2015).

748 **Figure 5:** Photomicrographs of **(a)** a glassy melt inclusion from a Thai ruby, **(b)** a recrystallized melt
749 inclusions from a Thai ruby, **(c)** a glassy melt inclusion from a Yogo sapphire, and **(d)** a recrystallized melt
750 inclusion from a Yogo sapphire

751 **Figure 6:** Oxygen isotope compositions and trace elemental compositions of seven Yogo sapphires (in
752 blue) and two reddish-violet Yogo sapphires (in red). The data for the trace element and oxygen isotope
753 comparisons were from pairs of spots placed as close as possible to each other in an attempt to sample

754 nearly the same volume. **(a)** shows 2 core and rim spots only, and **(b–d)** contains core and rim spots of
755 all nine Yogo samples, and additional core to rim traverses (5 spots) in four sapphires and one ruby.

756 **Figure 7:** Melting relations in the quartz (Qz) – anorthite (An) – forsterite (Fo) ternary at 2.0 GPa from Liu
757 and Presnall (1990). Bulk compositions for two hypothetical protoliths for Thai/Cambodian rubies and
758 Yogo sapphires are marked by the red and blue circles. Dashed red and blue lines show the evolution of
759 the two hypothetical protoliths during partial melting and demonstrate that corundum can be formed
760 through a peritectic melting reaction in this system. Red and blue stars mark the appearance of
761 corundum during partial melting.

762

This is a preprint, the final version is subject to change, of the American Mineralogist (MSA)
Cite as Authors (Year) Title. American Mineralogist, in press.
DOI: http://dx.doi.org/10.2138/am-2018-6164

Table 1: Trace element chemistry of rubies from Thailand and Cambodia and rubies and sapphires from Yogo Gulch, Montana, USA[1]

	Mg ppmw	Ti ppmw	V ppmw	Cr ppmw	Fe ppmw	Ga ppmw	Ga/Mg	Ga*/Al[2]	Cr/Ga	Fe/Ti
Thailand	150	148	22	2801	2986	26	0.18	0.50	107.5	21.3
	(118-206)	(95-210)	(16-33)	(450-7761)	(2454-3620)	(18-34)	(0.13-0.22)	(0.35-0.65)	(13.4-237.1)	(14.0-29.2)
Cambodia	129	136	19	1971	2957	24	0.19	0.45	85.0	23.4
	(102-163)	(81-219)	(9-30)	(955-2856)	(2175-3794)	(16-32)	(0.12-0.27)	(0.30-0.60)	(35.4-146.5)	(14.2-41.0)
Yogo	128	215	30	1749	3219	47	0.37	0.88	40.9	15.2
	(89-172)	(135-301)	(4-84)	(2-12590)	(2026-6631)	(31-80)	(0.20-0.57)	(0.58-1.51)	(0.06-307.88)	(8.6-28.2)
Detection Limits	0.01	0.3	0.03	0.5	2.4	0.03	-	-	-	-

1. Averages are shown at the top of each row and the range is shown below in parentheses. Analyses are for 14 rubies from Pailin, Cambodia, 10 rubies from Chantaburi-Trat, Thailand, and 44 rubies and sapphires from Yogo Gulch, Montana, USA.
2. Ga*/Al = Ga×10,000/Al

This is a preprint, the final version is subject to change, of the American Mineralogist (MSA)
Cite as Authors (Year) Title. American Mineralogist, in press.
DOI: http://dx.doi.org/10.2138/am-2018-6164

Table 2: Compositions of the melt inclusions (MI's) from blue sapphires and one reddish-violet sapphire from Yogo Gulch, MT, USA, one ruby from Thailand, and one ruby from Cambodia.

wt%	Yogo blue sapphire MIs remelted[a]	Yogo reddish-violet sapphire MI[b]	Thai ruby MI[b]	Cambodian ruby MI[b]
SiO_2	54.5	60.5	55.0	53.4
TiO_2	0.4	0.4	0.1	0.2
Al_2O_3	21.7	20.6	24.0	23.6
FeO	1.5	0.8	1.2	1.6
MgO	1.2	0.4	1.9	1.4
CaO	5.4	5.3	6.2	4.9
Na_2O	4.6	4.3	5.2	4.4
K_2O	1.7	1.0	0.1	3.1
volatiles	9.0	6.7	6.3	7.5

[a]Four averaged melt inclusions from Palke et al. (2016)
[b]One melt inclusion each for reddish-violet Yogo sapphire and Thai and Cambodian ruby

This is a preprint, the final version is subject to change, of the American Mineralogist (MSA)
Cite as Authors (Year) Title. American Mineralogist, in press.
DOI: http://dx.doi.org/10.2138/am-2018-6164

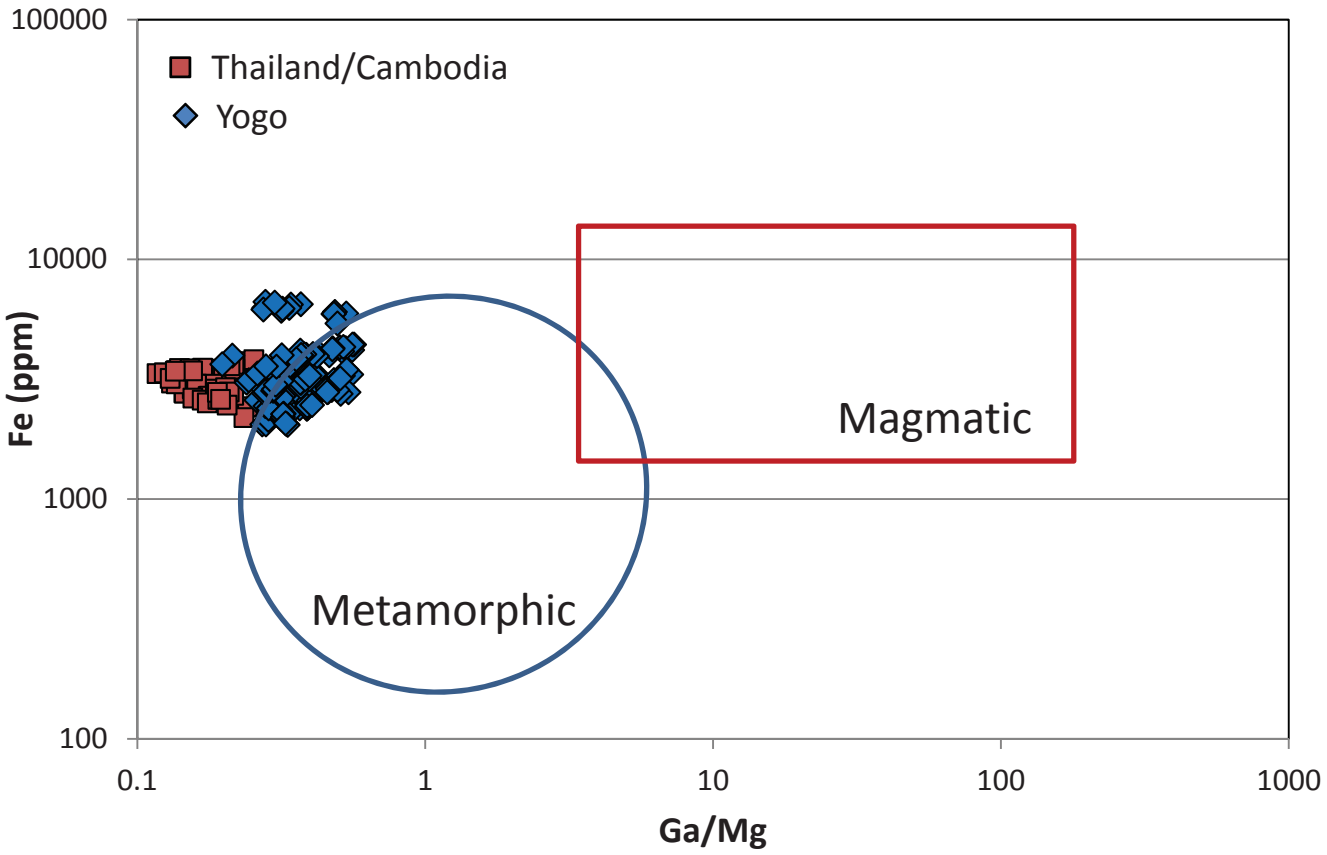

Figure 1

This is a preprint, the final version is subject to change, of the American Mineralogist (MSA)
Cite as Authors (Year) Title. American Mineralogist, in press.
DOI: http://dx.doi.org/10.2138/am-2018-6164

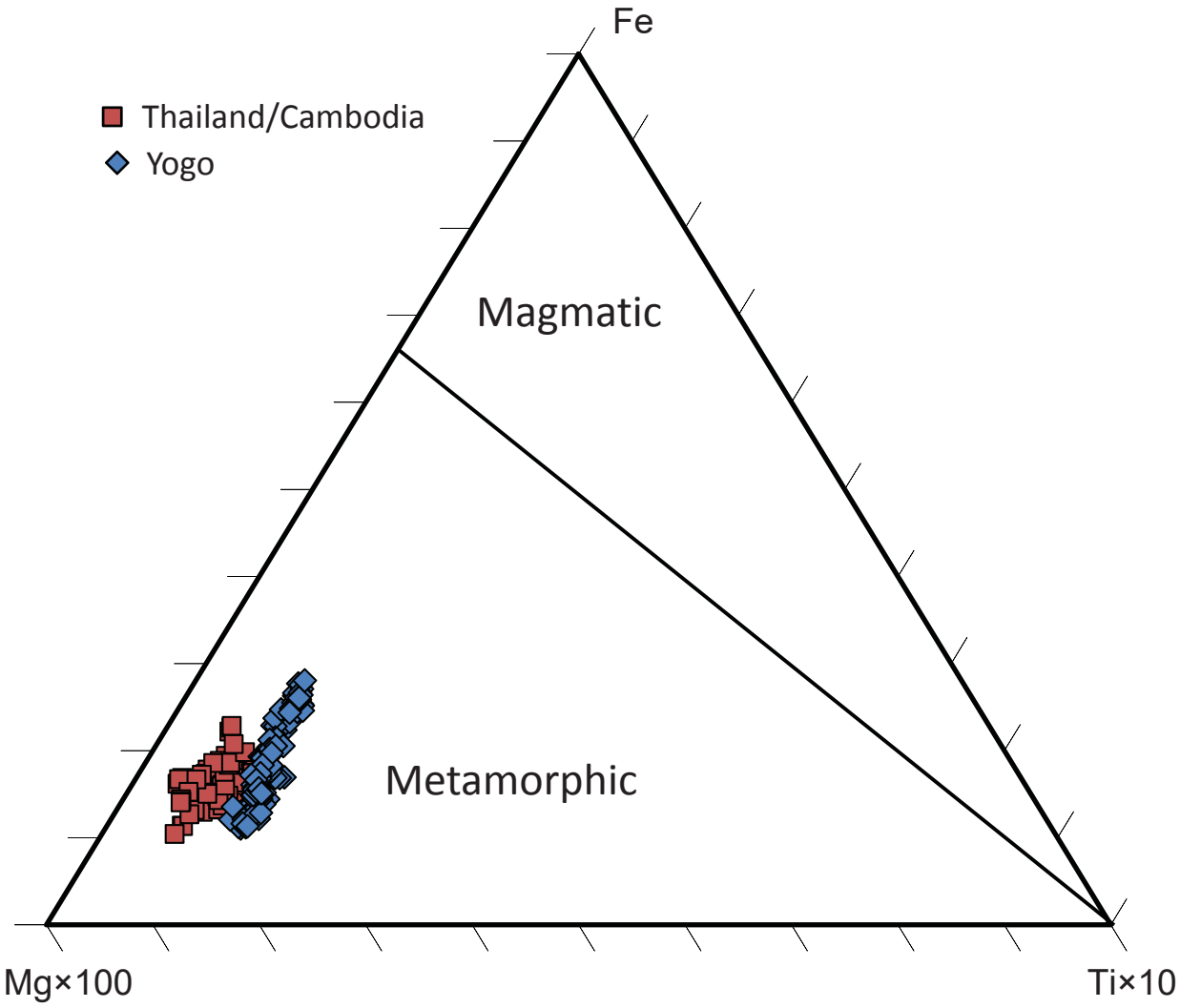

Figure 2

This is a preprint, the final version is subject to change, of the American Mineralogist (MSA)
Cite as Authors (Year) Title. American Mineralogist, in press.
DOI: http://dx.doi.org/10.2138/am-2018-6164

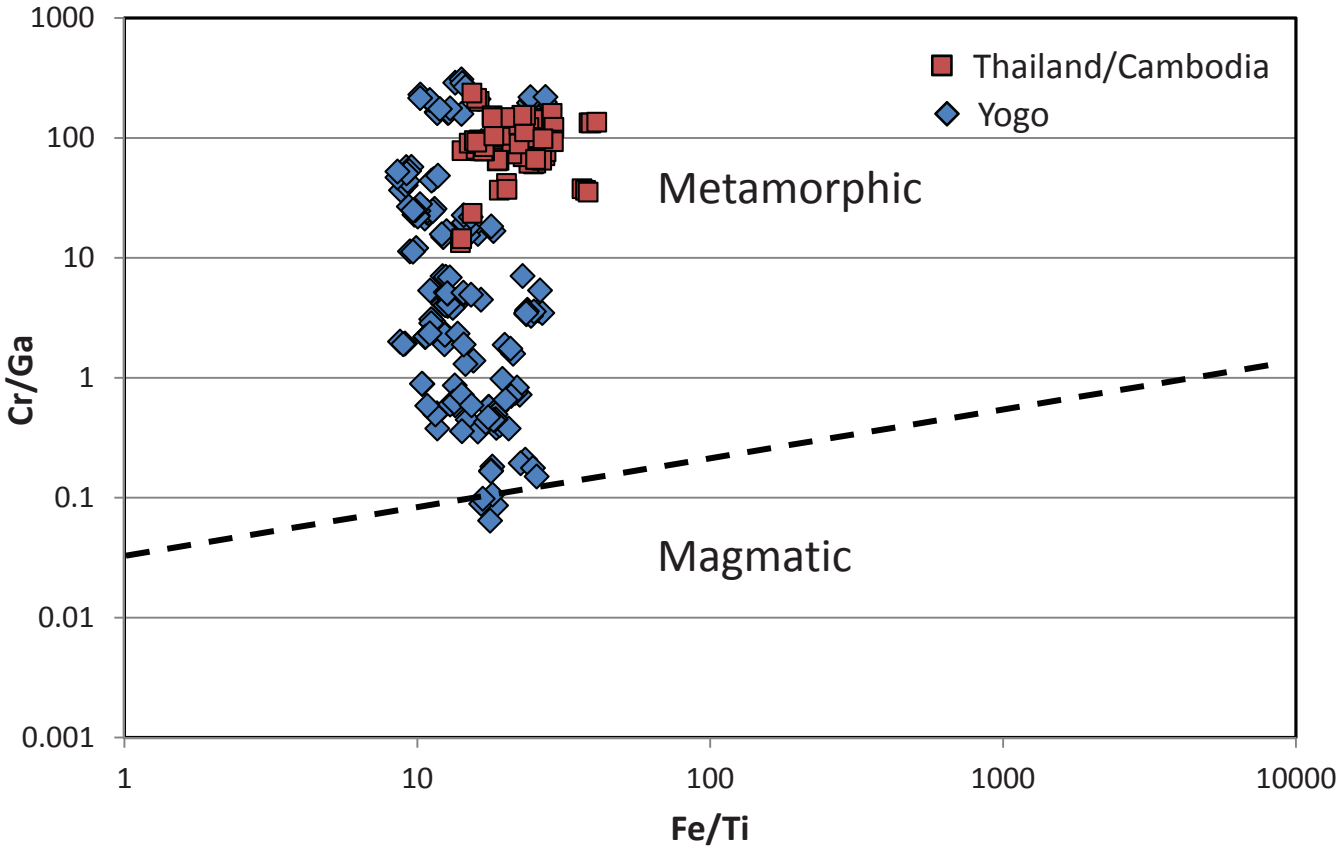

Figure 3

This is a preprint, the final version is subject to change, of the American Mineralogist (MSA)
Cite as Authors (Year) Title. American Mineralogist, in press.
DOI: http://dx.doi.org/10.2138/am-2018-6164

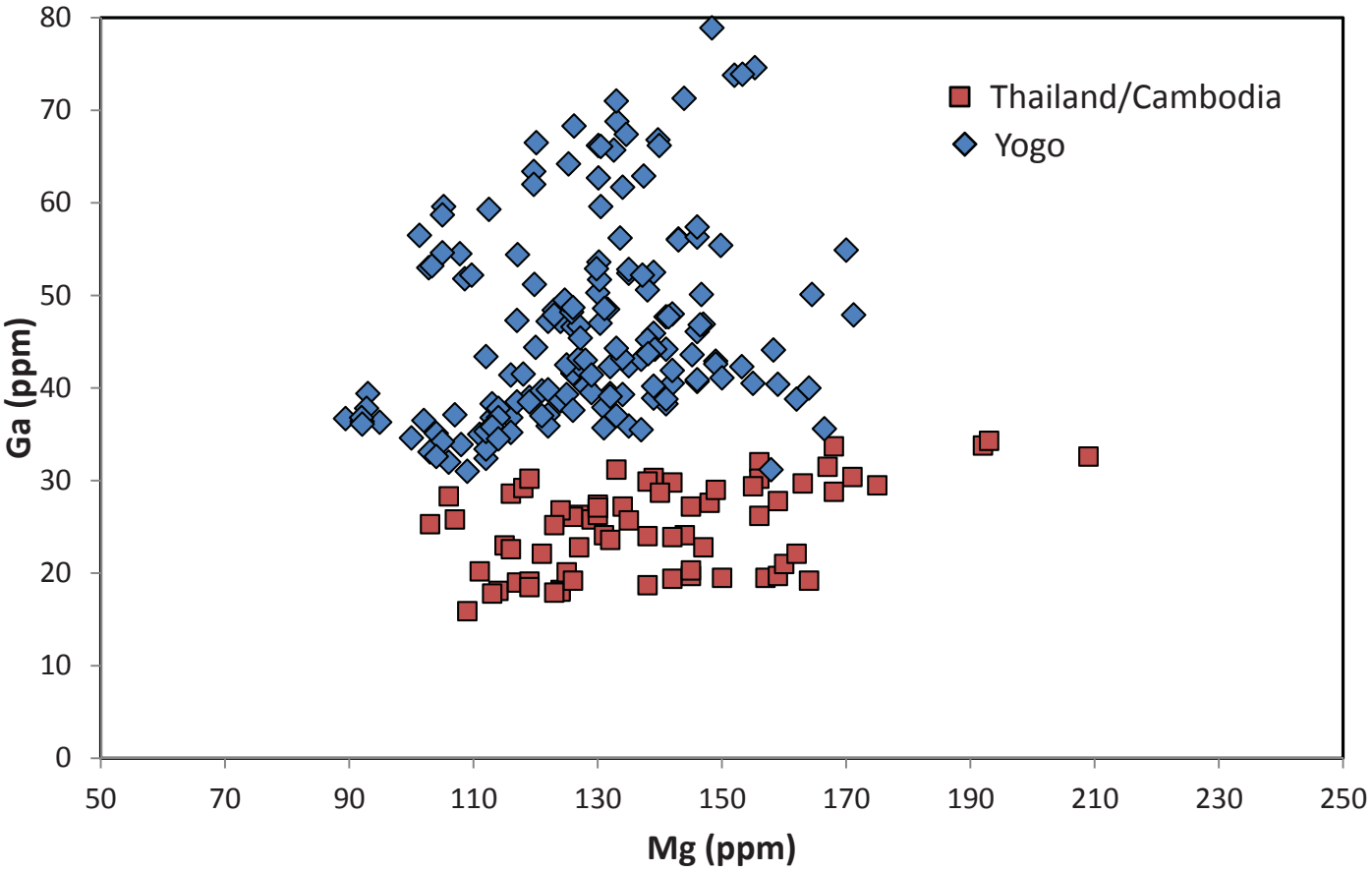

Figure 4a

This is a preprint, the final version is subject to change, of the American Mineralogist (MSA)
Cite as Authors (Year) Title. American Mineralogist, in press.
DOI: http://dx.doi.org/10.2138/am-2018-6164

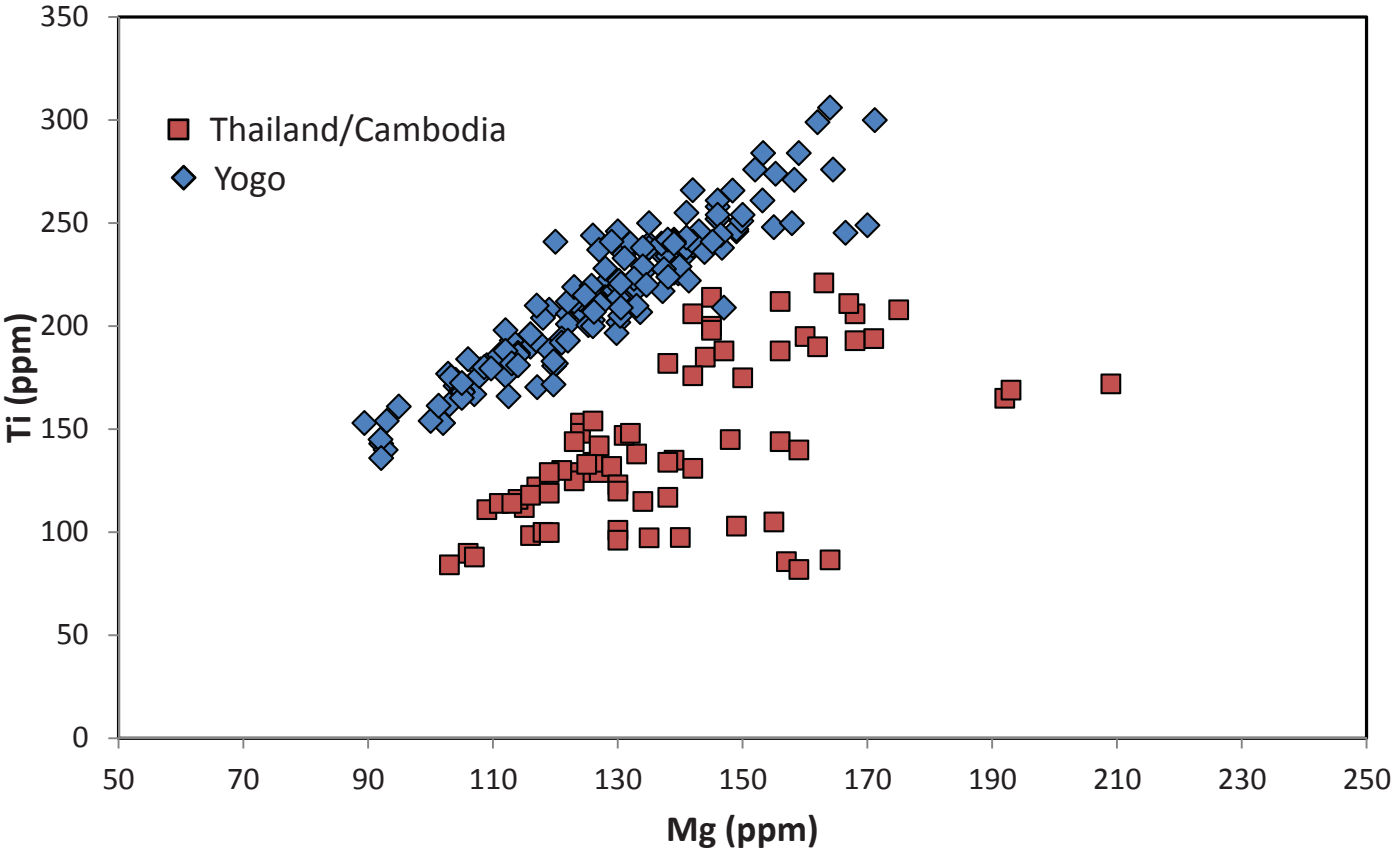

Figure 4b

This is a preprint, the final version is subject to change, of the American Mineralogist (MSA)
Cite as Authors (Year) Title. American Mineralogist, in press.
DOI: http://dx.doi.org/10.2138/am-2018-6164

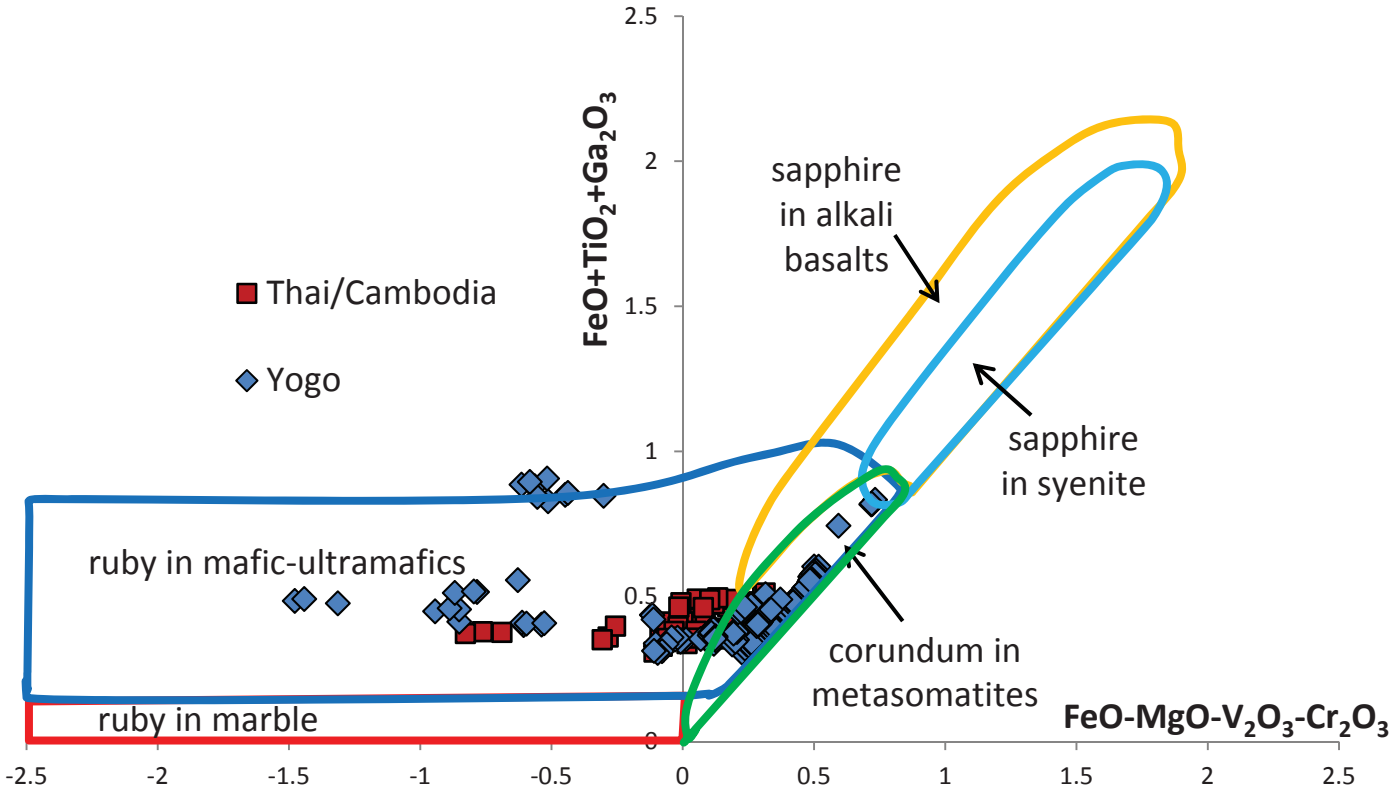

Figure 4c

This is a preprint, the final version is subject to change, of the American Mineralogist (MSA)
Cite as Authors (Year) Title. American Mineralogist, in press.
DOI: http://dx.doi.org/10.2138/am-2018-6164

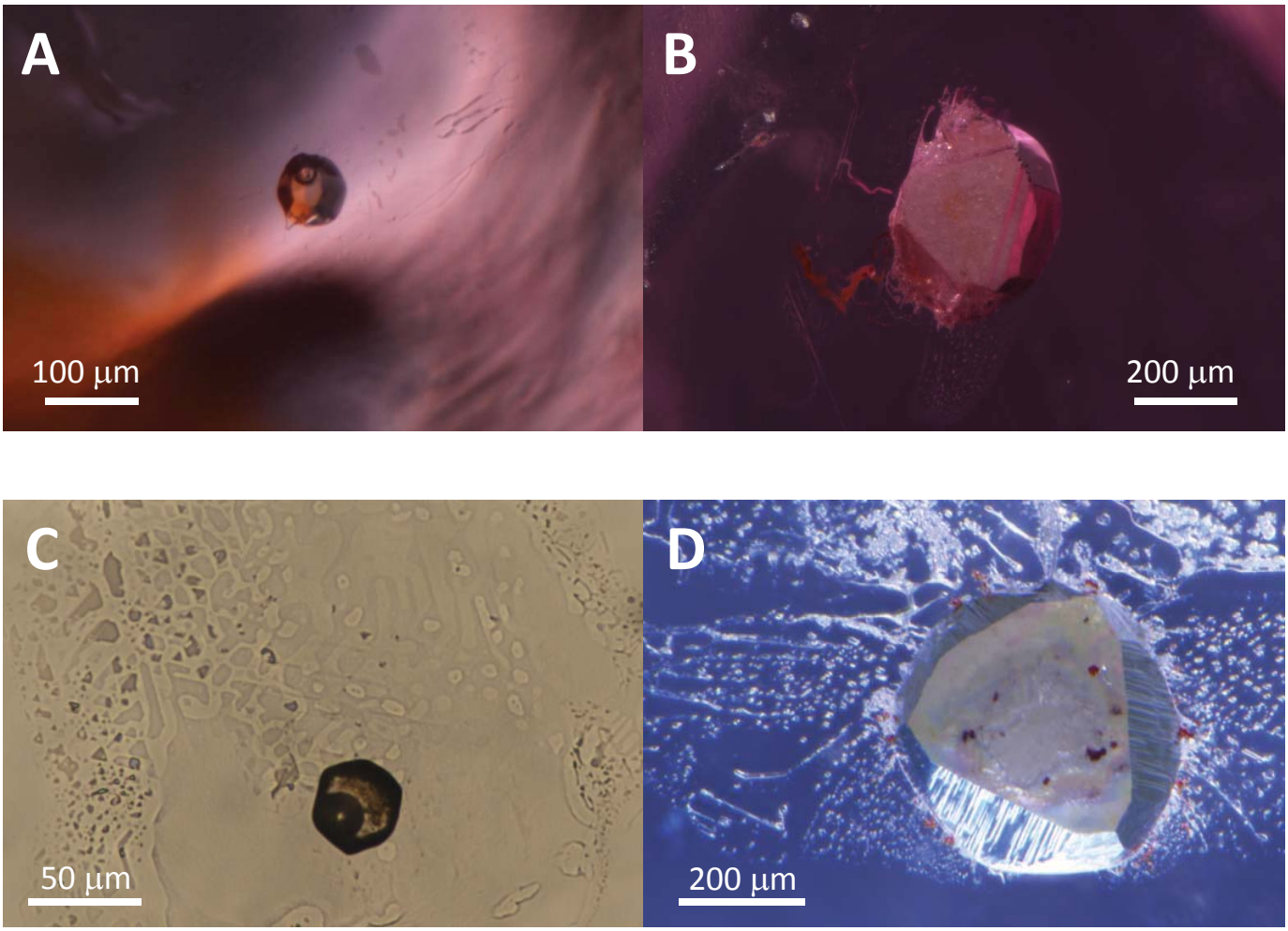

Figure 5

This is a preprint, the final version is subject to change, of the American Mineralogist (MSA)
Cite as Authors (Year) Title. American Mineralogist, in press.
DOI: http://dx.doi.org/10.2138/am-2018-6164

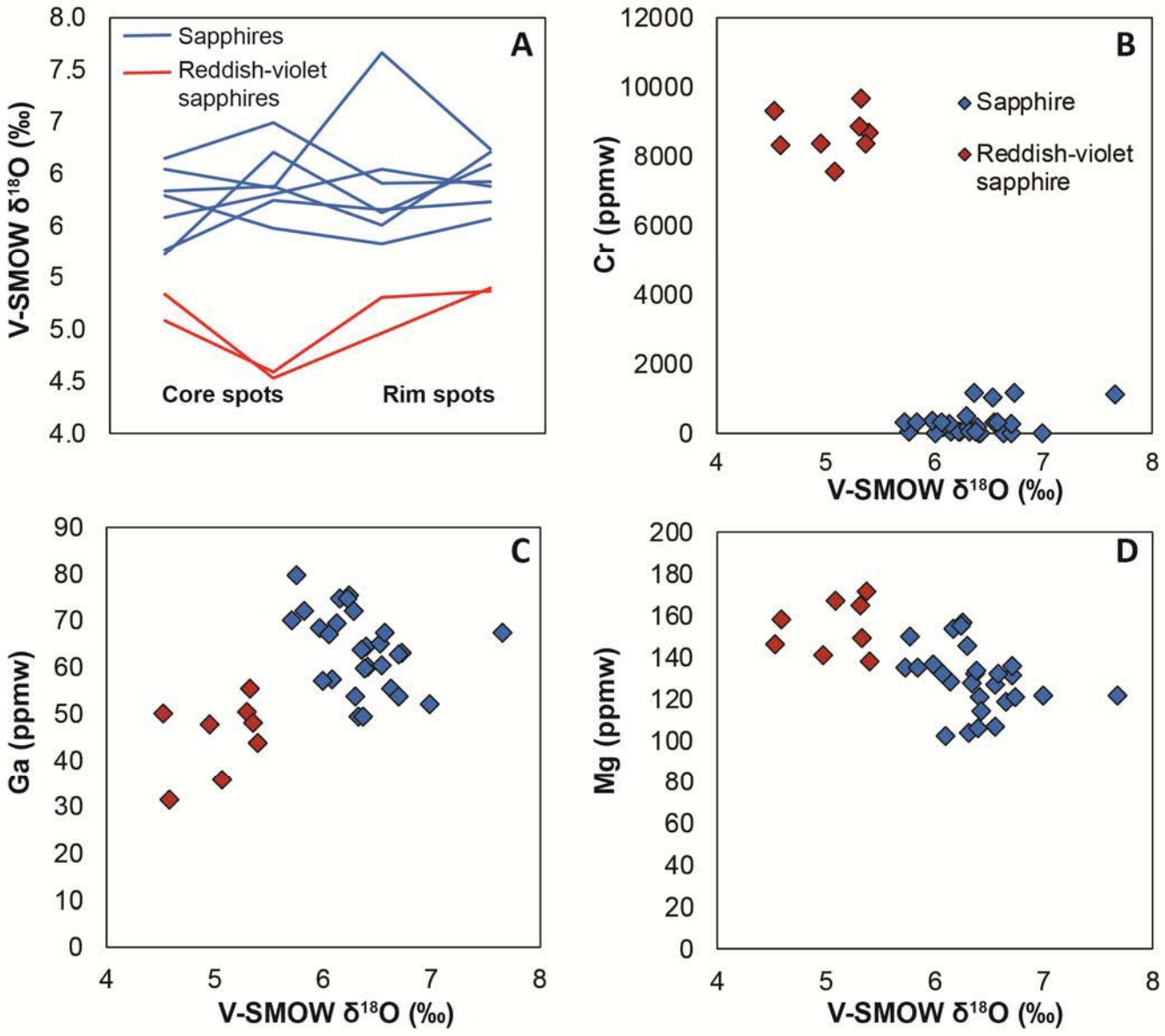

Figure 6

This is a preprint, the final version is subject to change, of the American Mineralogist (MSA)
Cite as Authors (Year) Title. American Mineralogist, in press.
DOI: http://dx.doi.org/10.2138/am-2018-6164

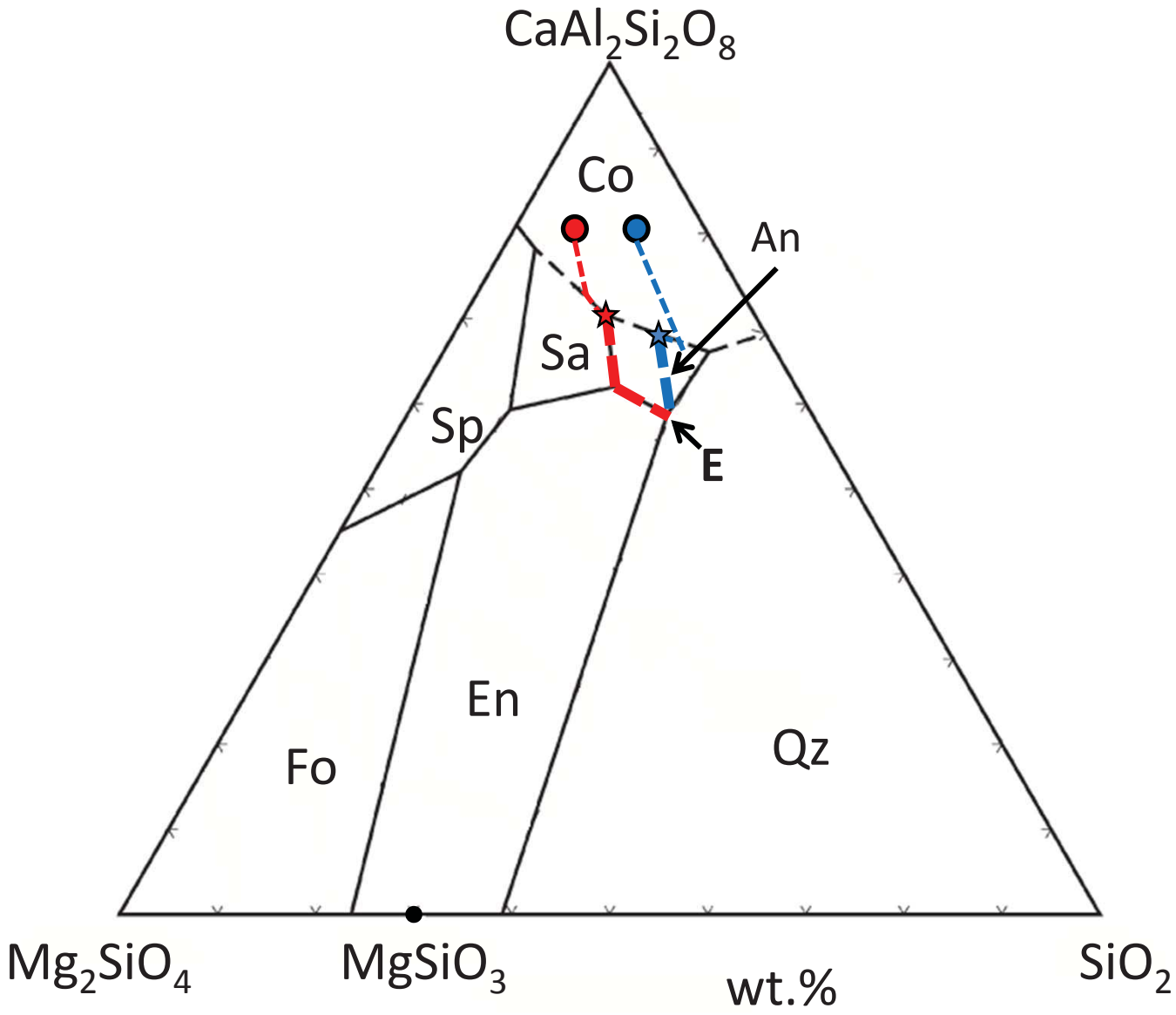

Figure 7